Carrier relaxation and recombination in GaAs/AlGaAs quantum heterostructures and nanostructures probed with time-resolved cathodoluminescence

H. T. Lin, D. H. Rich,[a] A. Konkar, P. Chen, and A. Madhukar

Photonic Materials and Devices Laboratory, Department of Materials Science and Engineering, University of Southern California, Los Angeles, California 90089-0241

We have examined the kinetics of carrier relaxation in GaAs/AlGaAs quantum wells (QWs), quantum wires (QWRs), and quantum boxes (QBs) with time-resolved cathodoluminescence (CL). In the cases of QWRs and QBs, the nanostructures were grown via a size-reducing growth approach on pre-patterned GaAs(001) substrates composed of stripes and mesas, respectively. The growth involved deposition of multiple GaAs/AlGaAs layers in order to establish both structural and optical markers which facilitated the identification of important features in transmission electron microscopy (TEM) and CL experiments. In TEM measurements, the lateral dimensions of the top-most GaAs layers in typical stripe and mesa structures comprising the QWRs and QBs delineate GaAs regions expected to exhibit 2D and 3D quantum confinement effects, respectively. Time-delayed CL spectra of all three structures reveal that the initial capture of carriers in the active regions occurs on a time scale less than the temporal resolution of the CL system, ~ 100 ps, during the onset of luminescence. Hot carriers, as a result of re-emission out of thin QWs surrounding the QWRs and QBs, exhibit diffusive transport followed by relaxation into laterally confined regions which exhibit confined states of lower energy. This thermalization gives rise to a relatively slow onset and decay of luminescence attributed to the lowest energy optical transitions. By comparing time-resolved CL transients in these three structures, we find that the average luminescence onset and initial-decay rates both decrease as the dimensionality of the system reduces from 2D to 0D. These results demonstrate that the rate of carrier relaxation, including the re-emission and diffusive transport of carriers, will depend on details of the *total* surrounding structure which comprises the excitation region. © *1997 American Institute of Physics.* [S0021-8979(97)05407-8]

I. INTRODUCTION

Optically active nanostructures (quantum wires and boxes) have attracted much attention recently. Among their several interesting properties, they possess enhanced nonlinear optical properties[1] which are important for applications in optical communication that involve switching, amplification, and signal processing. Among the techniques used to fabricate nanostructures, size-reducing epitaxial growth approaches which utilize the dependence of cation migration rates on the crystallographic facet orientation,[2–6] have been a subject of much activity. The high quality of the heterolayers and interfaces that can be achieved during an *in situ* single growth step circumvents the need for post-growth processing (e.g., conventional lithography, wet, and dry chemical etching) on a nanoscale that can inevitably degrade the optical and structural quality of the nanostructure and its surrounding barriers. A number of efforts have succeeded in employing single step growth approaches for the fabrication of GaAs/$Al_xGa_{1-x}As$ nanostructures.[2–6] Such size-reducing growth not only facilitates the fabrication of well-defined periodic nanostructure arrays, but also facilitates the study of the optical properties of isolated nanostructures. Nanostructures residing in close proximity to each other (i.e., less than the carrier diffusion length) could result in a more complex environment in which the excited electrons and holes interact with several nanostructures, as in the cases for the growth of self-organized InAs islands[7–9] and strain-induced laterally ordered (SILO) $(InP)_2/(GaP)_2$ quantum wires (QWRs).[10,11] A fundamental issue concerning laser applications is the tailoring of the nanostructures to achieve an optimum quantum capture and collection efficiency. Using time-resolved cathodoluminescence (CL), we have previously studied the kinetics of carrier relaxation in GaAs/AlGaAs layers grown on a pre-patterned GaAs(001) substrate via a size-reducing growth technique, and showed evidence for thermal re-emission of carriers from thinner quantum wells (QWs), diffusive transport of carriers across $Al_xGa_{1-x}As$ barriers, and carrier collection into 3D confined GaAs regions, i.e., quantum boxes (QBs).[12] In this paper, we have further extended our studies of the carrier relaxation kinetics in QWs, QWRs, and QBs in an attempt to better understand the impact of size reducing growth on the carrier capture and collection efficiency in nanostructures.

II. EXPERIMENT

A. Sample preparation

The details of the sample preparation and procedure for substrate encoded size-reducing molecular beam epitaxial growth have been previously reported for the growth of 3D confined GaAs volumes on GaAs(111)B and GaAs(001) substrates.[2–4] For this study, GaAs(001) substrates were pat-

[a]Author to whom correspondence should be addressed. Electronic mail: danrich@alnitak.usc.edu
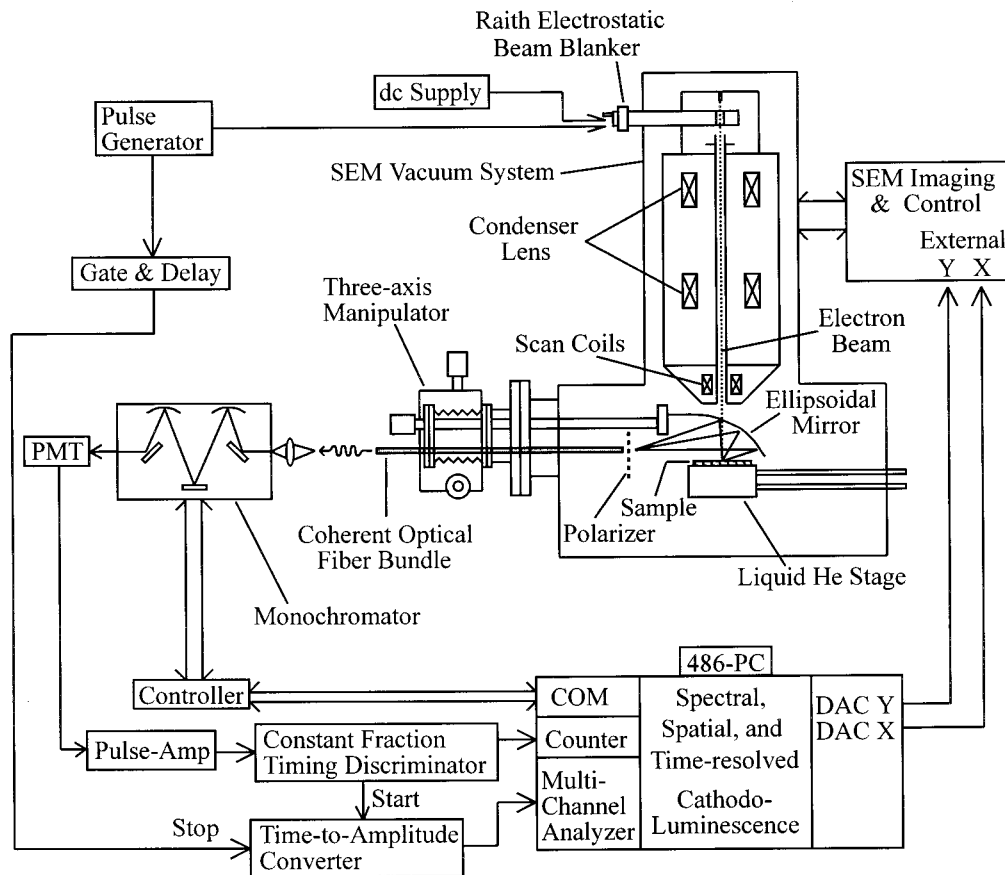
FIG. 1. Schematic diagram of the low-temperature time-resolved CL setup attached to a JEOL 840-A SEM. For high spectral-resolution CL spectroscopy measurements, the monochromator and PMT are replaced by a spectragraph and a LN cooled CCD array detector.

terned along $\langle 100 \rangle$ directions using conventional photolithography followed by wet chemical etching to give (i) square mesas and (ii) long stripes with ~ 3–4 μm in width and ~ 2–3 μm in vertical height. Samples prepared with procedures (i) and (ii) are, hereafter, simply referred to as mesas and stripes which result in the formation of QB and QWR arrays, respectively. The growth consisted of a size-reducing buffer layer consisting of four periods of 175 ML $Al_{0.25}Ga_{0.75}As$/525 ML GaAs followed by a 40 period multiple quantum well (MQW) composed of 40 ML $Al_{0.25}Ga_{0.75}As$/20 ML GaAs (1 ML=2.83 Å). During the size-reducing growth, the Ga adatoms migrate from the sidewalls toward the mesa (stripe) top, yielding a higher growth rate on the mesa (stripe) top than on the adjacent sidewalls.[2–4] A TEM examination of this growth showed that the (001) surface layers are laterally bounded by {101} facets on the stripe sidewalls. The evolution of the growth on the mesa sidewalls involves the formation of {103} and {101} facets bounding the (001) surface layers on the mesa top.

B. Time-resolved cathodoluminescence setup

A detailed schematic diagram of the low-temperature CL setup based on a modified JEOL-840A scanning electron microscope (SEM) is shown in Fig. 1. A continuous-flow liquid He cryogenic stage, allowing for a temperature control between 15 and 300 K, was implemented. A custom designed

optical collection system composed of an ellipsoidal mirror, a three-axis manipulator, and a coherent optical fiber bundle was attached to the SEM vacuum chamber in order to collect and transmit the optical signal. The light emitted by the injection of high-energy electrons (500 V–40 keV) into samples is then dispersed by (i) a 1/4 m monochromator followed by detection with a cooled Cs:GaAs photomultiplier tube (PMT) for the time-resolved CL measurements in photon counting mode or (ii) a 0.275 m spectrograph followed by detection with a liquid nitrogen (LN) cooled CCD array detector for high-spectral-resolution spectroscopy measurements. To perform linearly polarized CL measurements (LPCL),[13] a rotatable vacuum linear polarizer was mounted directly in front of the fiber bundle. A Raith electrostatic beam-blanking unit is located directly below the electron gun; e-beam pulses with rise and decay times of ~ 100 ps, a variable width of 5–140 ns, and a repetition rate of 100 Hz to 1 MHz can be used for excitation of the samples.

The block diagram of the time-correlated single photon counting system using the method of delayed coincidence is shown in Fig. 2. The anode signal from PMT was amplified by a fast timing pre-amplifier, ORTEC Model VT120, and fed into a constant fraction differential discriminator, ORTEC Model 583, to allow an optimum timing output. In the constant fraction technique, an input reference signal to the constant fraction circuitry is delayed in accordance with
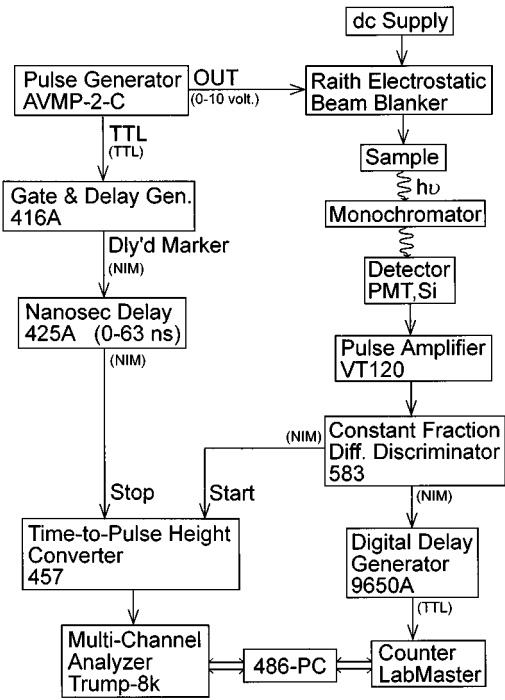
FIG. 2. Time-resolved CL instrumentation showing scheme for time-correlated single photon counting using the method of delayed coincidence in an inverted single photon counting mode.

FIG. 3. The timing configuration of the delayed coincidence scheme for CL decay measurements.

the input signal. A fraction of the undelayed pulse is subtracted from the input signal, generating a bipolar signal in which the zero crossing occurs at the same fraction of the input pulse height regardless of the amplitude of the input signal. The zero crossing signal provides the timing output which is then (i) buffered by a digital delay generator, EG&G Model 9650A, to allow conversion into a TTL pulse for direct photon counting or (ii) fed into a time-to-pulse height converter, ORTEC Model 457, to serve as the start pulse for the delayed coincidence in an inverted single photon counting mode. The pulse generator (AVTECH Model AVMP-2-C), which triggers the beam-blanking unit, also triggers a gate and delay generator, ORTEC Model 416A, using a separate TTL output. A NIM-standard delayed marker signal is then fed into an ORTEC 425A delay module for an additional delay in 1-ns steps from 1.7 to 64.7 ns. The delayed NIM-standard signal serves as the stop pulse for the time-to-pulse height converter. The time interval between the start and stop pulses is then measured via an analog output pulse having a voltage proportional to the measured time difference. The pulse height distribution is measured by a PC-486 computer controlled multichannel analyzer (MCA), an ORTEC Trump-8k card which is a system usually employed for energy-dispersive x-ray analysis. The pulse height distribution is proportional to the probability distribution for photon emission in the measured time range, provided the total photon count rate is much less than the repetition rate. In the inverted mode, unconsummated starts are avoided which reduces the dead time and leads to a more efficient use of the MCA electronics. Figure 3 shows a pulse timing diagram of the CL signal, i.e., a photon event and controlled delay used to implement the CL delayed coincidence
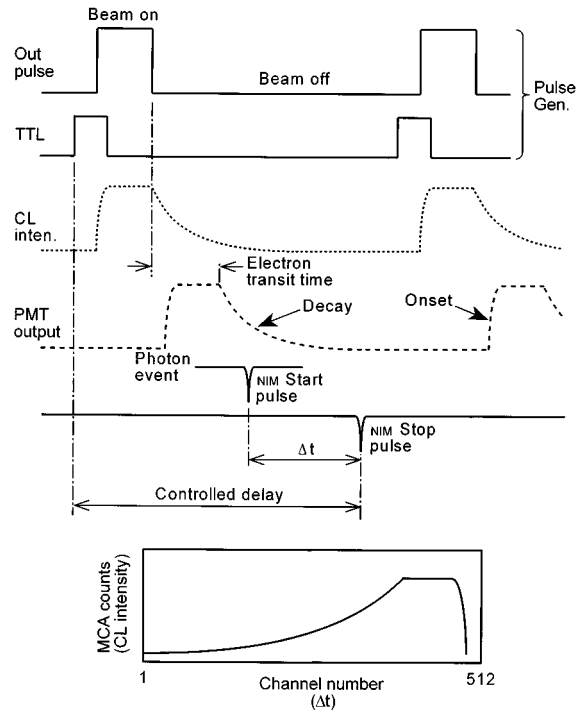
scheme. The controlled delay, i.e., the NIM stop pulse with respect to the TTL signal of the pulse generator, was adjusted to account for the PMT transit time (in general, tens of ns), instrumentation delay, and to select the detected time range of interest. Time-delayed CL spectra at different time windows with respect to the beginning and end of the excitation pulse (i.e., the onset and decay stages, respectively) can be simultaneously acquired under the same experimental conditions with a temporal resolution of ~ 100 ps; without the need for repetitive wavelength scans.

III. RESULTS AND DISCUSSION

A. Constant excitation CL spectroscopy and imaging

Results of constant excitation CL spectroscopy are shown in Fig. 4 for the planar, stripe, and mesa top regions. The CL spectra were taken with the beam rastered about a ~ 1 μm $\times 1$ μm area with the stripe and mesa tops positioned at the center in the cases for those regions, yielding a spatial average over those regions. The CL spectrum of a planar region shows a sharp peak at $\lambda \approx 782$ nm, corresponding to the first quantized e1-hh1 excitonic transition in the GaAs/Al$_{0.25}$Ga$_{0.75}$As MQWs at $T = 87$ K. The cross-sectional TEM images of typical planar, stripe, and mesa regions are shown in Figs. 5(a), 5(b), and 5(c), respectively. The measured GaAs QW thickness in the planar region is ~ 50 Å, which is in reasonable agreement with the nominal thickness of 20 ML from the growth. The pinch-off regions in both the stripe and mesa are identified by the arrows in Figs. 5(b) and 5(c), which show the top most (001) GaAs layers prior to the shrinkage of stripe and mesa to a wedge and an apex, respectively. Evidently, an increase in the QW and barrier thickness of the (001) layers relative to the as-deposited MQW in
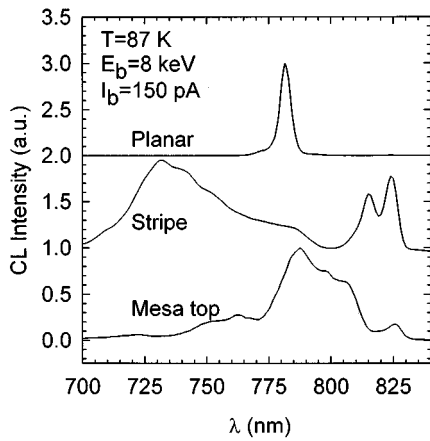
FIG. 4. Constant excitation CL spectra for planar, stripe, and mesa regions at $T=87$ K. The CL spectra were taken with the beam rastered about an $\sim 1~\mu$m$\times 1~\mu$m region to give a spatial average over this region.
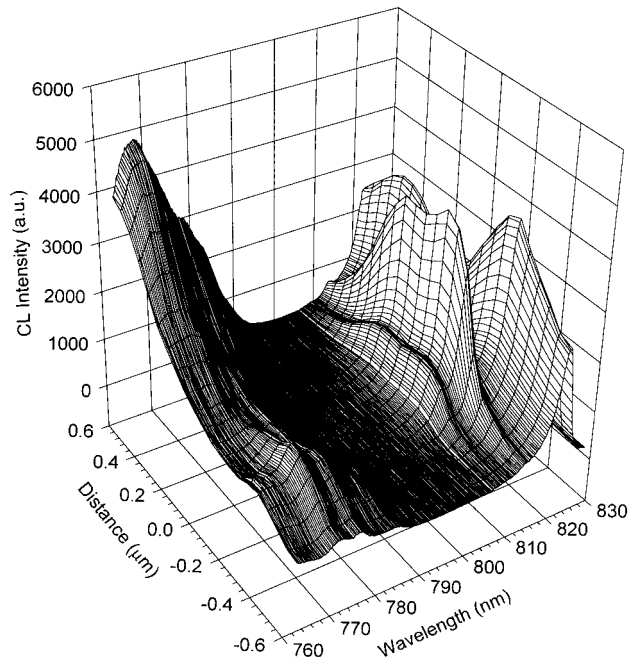
FIG. 6. Local CL spectra in the wavelength range 760 nm$\leqslant\lambda\leqslant$830 nm at regions in varying proximity to the stripe center.
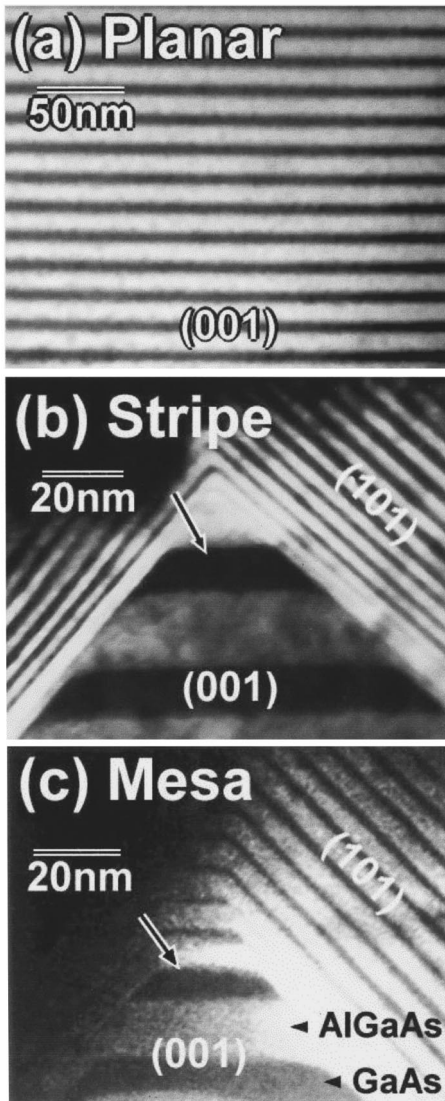
FIG. 5. Cross-sectional TEM images of planar, stripe, and mesa regions.

the planar region is observed in Figs. 5(b) and 5(c), as a result of the interfacet cation migration and facet-dependent growth rates. The TEM shows a trapezoidal shape for the top-most (001) GaAs volumes, as indicated by the arrows in Figs. 5(b) and 5(c). The corresponding dimensions for the height, base, and top are 120, 500, and 280 Å, for the stripe region and 100, 440, and 275 Å for the mesa region, thereby demonstrating GaAs regions expected to exhibit quantum confinement effects. Subsequent growth after pinch-off resulted in a ~ 0.2-μm-thick short period GaAs/AlGaAs MQW for the stripe and mesa on the sidewalls whose well width, w, varies mainly from ~ 10–50 Å.

For the stripe and mesa regions, the enhanced growth on GaAs (001) surface layers prior to pinch-off is expected to yield a luminescence spectrum with its peak wavelength red-shifted. For both samples, the growth on the sidewalls yielded thinner QW layers from TEM, resulting in a spectral blue-shift. For the CL spectrum in the stripe region as shown in Fig. 4, we identify the intense broad luminescence with peak centered at ~ 732 nm with the luminescence from the GaAs/AlGaAs MQW sidewalls. A distinct peak at ~ 815 nm in the stripe CL spectrum represents the luminescence from the thick GaAs/AlGaAs QWs that formed just prior to the pinch-off. The peak at ~ 825 nm is identified as emission from the underlying GaAs/AlGaAs size-reducing buffer layer. Stack plots of local CL spectra for the wavelength range 760 $\leqslant\lambda\leqslant$830 nm at regions in varying proximity to the stripe center are shown in Fig. 6. It is evident that the sidewalls are responsible for the luminescence of shorter wavelength $\lambda\leqslant 800$ nm. The emission at $\lambda=815$ nm reaches its maxima on both sides of the stripe at about 0.12 μm away from the stripe center. Such a distance is much smaller than the carrier diffusion length which is on the order of μm. Therefore, a small intensity drop at the stripe center, located

J. Appl. Phys., Vol. 81, No. 7, 1 April 1997

Lin *et al.* 3189

between two luminescence maxima, is likely due to a variation of the excitation density and carrier collection at the top of the stripe. Due to the geometry of the sidewalls, an enhanced transport of carriers to the wedge region may occur when the e-beam is displaced slightly away from the center of the stripe. Also, the buffer layer exhibits a luminescence intensity maxima for $\lambda = 825$ nm on both sides; the maxima are ~ 0.3 μm away from the center of the stripe. These results show that the geometry of the wedge, for a vertically injected e-beam, will influence the local excitation rates and subsequent carrier collection into the wedge.

A fundamental optical property associated with 2D quantum confined nanostructures (i.e., quantum wires) is the presence of a polarization in the excitonic luminescence emitted from the QWR.[14] The luminescence emitted from the lowest energy excitonic transitions in unstrained QWRs is partially polarized along the QWR axis.[15] The polarization anisotropy present in excitonic luminescence from QWRs has been used to evaluate the relative structural quality of the QWR.[16,17] In order to further assess the nature of 2D quantum confinement, we have examined the polarization properties of luminescence emitted from the stripe samples for the luminescence identified as QWR emission at $\lambda \approx 815$ nm. Linearly polarized CL measurements were performed for light detected with the electric field **E** parallel and perpendicular to the stripe. The results of local CL spectra for the wavelength range $800 \leqslant \lambda \leqslant 830$ nm at regions in varying proximity to the stripe center are shown in Figs. 7(a) and 7(b) for light with electric field **E** polarized parallel and perpendicular to the [100]-oriented stripe (i.e., **E**∥[100] and **E**⊥[100]), respectively. By comparing Figs. 7(a) and 7(b), it is apparent that for the **E**∥[100] case, the luminescence in the vicinity of the stripe center (distance = 0) exhibits a local enhancement of intensity by $\sim 7\%$ for the emission in the $810 \leqslant \lambda \leqslant 815$ nm range. These results exhibit fundamental optical properties associated with a QWR behavior and underscore the viability of utilizing size-reducing growth to achieve true QWR structures.

For the CL spectra in the mesa regions, as shown in Figs. 4 and 8, three identifiable peaks, labeled $p1$-$p3$, are observed to lie within the intense broad luminescence feature located in the $780 \leqslant \lambda \leqslant 815$ nm range for $T = 87$ K; a fourth peak, $p4$, has its peak emission at 826 nm and is identified as emission from the underlying 525 ML GaAs buffer layers. Peaks $p1$-$p3$ are observed to follow the shift of the GaAs peak with temperature, and are expected to originate from the various GaAs/Al$_x$Ga$_{1-x}$As layers grown on the mesa. A SEM and various CL images for increasing wavelengths in the 763–826 nm range of this mesa are shown in Fig. 9. As observed in the CL imaging, emissions at different wavelengths have varying degrees of localization about the mesa top. Images in Figs. 9(b) and 9(c) show that the luminescence at 763 and 788 nm, respectively, is primarily from regions along the sidewalls away from the mesa top. As the wavelength increases from 798 to 814 nm, in Figs. 9(d)–9(f), we observe a greater localization of luminescence about the mesa top. Calculations of the $n=1$ electron to heavy-hole (e1-hh1) transition energy in Al$_{0.25}$Ga$_{0.75}$As/GaAs QWs at $T = 87$ K show that the $780 \leqslant \lambda \leqslant 815$ nm range corresponds to
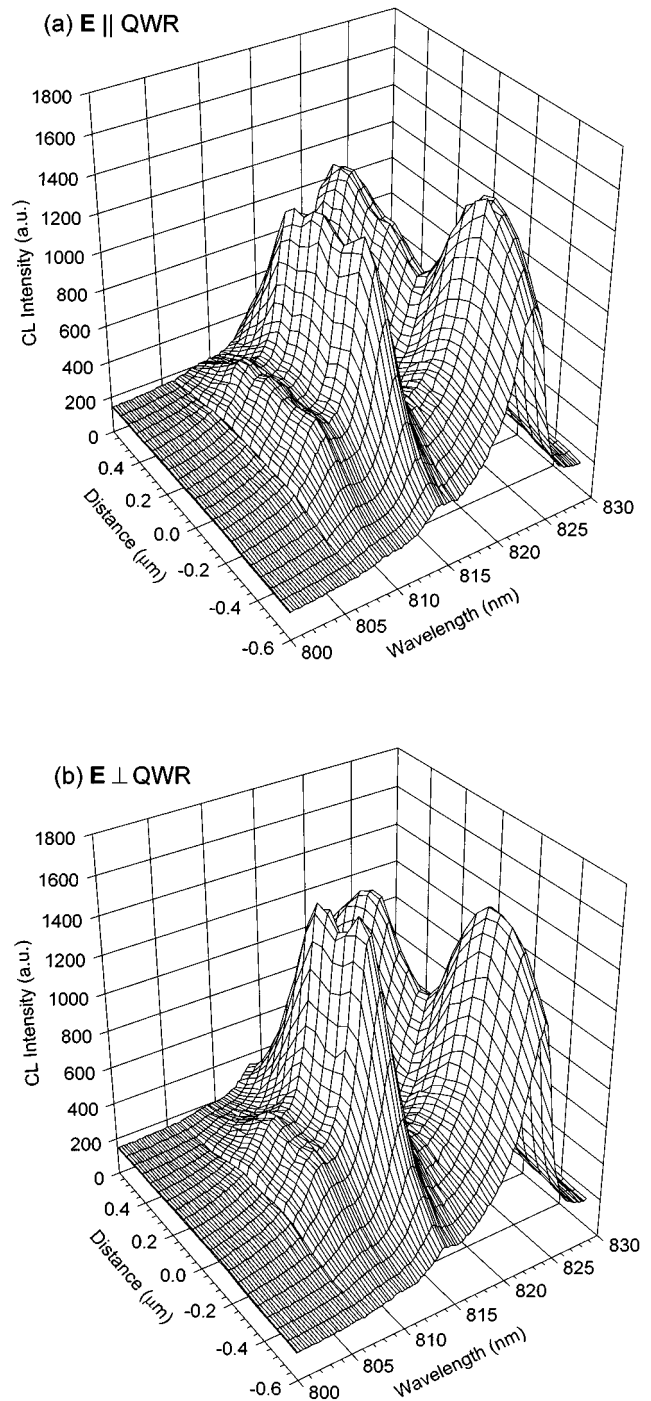
FIG. 7. Local CL spectra in the wavelength range 800 nm $\leqslant \lambda \leqslant 830$ nm at regions in varying proximity to the stripe center for light polarized (a) parallel and (b) perpendicular to the stripe.

QW widths in the $48 \leqslant w \leqslant 130$ Å range. Additional smaller peaks are observed in the $723 \leqslant \lambda \leqslant 760$ nm range, corresponding to $16 \leqslant w \leqslant 32$ Å. Thus, in connecting the CL observations with the aforementioned TEM measurements, we conclude that emission involving $\lambda \leqslant 800$ nm ($w \leqslant 75$ Å) is attributed to luminescence from the sidewall QWs, while emission in the $805 \leqslant \lambda \leqslant 815$ nm range originates from the thick ($90 \leqslant w \leqslant 130$ Å) QWs below the pinch-off region. These results are further supported by a CL depth-profiling
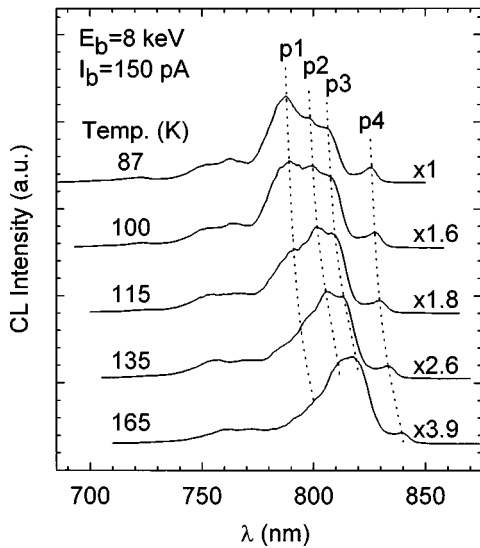
FIG. 8. Constant excitation CL spectra taken with various samples temperatures in the $87 \leqslant T \leqslant 165$ K range. The wavelength shift in peaks, $p1$-$p4$, with temperature is illustrated with the dashed lines.

FIG. 9. SEM (a) and monochromatic CL images at various wavelengths (b)–(g) of a typical mesa. The arrows in (b)–(g) point to the mesa top where pinch-off occurred. The length scale for images (b)–(g) is indicated in the SEM image. CL imaging parameters are indicated at the top of the figure.

measurement which shows a large increase in the $p3$ peak intensity relative to the $p1$ intensity as the beam energy, E_b, is increased from 1 to 10 keV.

Results of constant excitation CL spectroscopy, taken again with the beam rastered about an $\sim 1\,\mu\mathrm{m} \times 1\,\mu\mathrm{m}$ region centered at the mesa top, at various temperatures are shown in Fig. 8. For temperatures increasing from 87 to 165 K, the peak intensity of $p1$ decreases rapidly relative to that for $p3$, thereby revealing salient aspects concerning the thermalization of carriers. This is consistent with a larger thermal re-emission of carriers from thinner QWs relative to thicker QWs for this temperature range. Despite the large carrier capture rate in short period MQWs due to quantum capture,[18] the larger e1-hh1 energies in thinner QWs likewise reduce the barrier height for thermal re-emission,[19,20] leading to a considerable reduction in QW luminescence efficiency at these higher temperatures. The relative increase in $p3$ therefore suggests that these hot carriers are able to diffuse over sub-μm distances, thereby giving rise to carrier collection in the 3D confined regions, i.e., the QB, beneath the pinch-off layer.

B. Time-resolved CL measurements

In order to further examine the thermalization of carriers in close proximity to the nanostructures, time-delayed CL spectra at 87 K were obtained for the planar, stripe, and mesa regions, as shown in Fig. 10. All spectra are renormalized to have about the same maximum peak height. The time windows O6–O1 and D1–D5 denote time windows relative to the beginning of *onset* and *decay*, respectively, of the luminescence, as referred to the beginning and end of the electron beam pulses. The constant excitation spectra, which were measured in the center of the 50 ns excitation pulse, are labeled *in pulse* in Fig. 10.

For the planar region, both the emissions from the GaAs QW (p_{QW}) and buffer (p_{buffer}), i.e., $\lambda \approx 782$ and 825 nm,
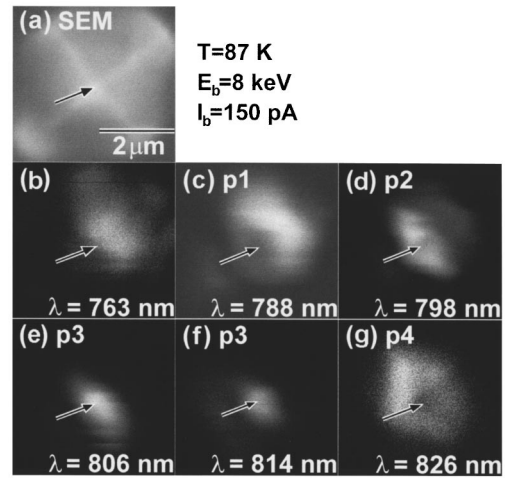
respectively, are clearly observed for the O6 time window centered at 150 ps due to initial carrier capture followed by recombination in GaAs QWs and buffer. The e1-hh1 excitonic luminescence from the GaAs QWs, p_{QW}, exhibits a visible blue-shift from $\lambda \approx 785$ nm to ~ 782 nm as the onset time windows progress from O6 to O4. This blue-shift is evidently a result of phase-space filling effects and attributed to a normal carrier collection from the AlGaAs barriers into the GaAs QWs. The rate at which p_{QW} blue-shifts, reflects the temporal evolution of carrier capture and recombination in GaAs QWs. In order to further study the temporal behavior, the initial onset and decay curves of p_{QW} were measured, as shown in Figs. 11(a) and 11(b), respectively. The onset rate r, which we define as $r = \Delta \ln(I_{\mathrm{CL}})/\Delta t$ and is given by the slope of the tangent to the onset curve of p_{QW} in Fig. 11(a), is 3.06 ns^{-1}. The initial luminescence decay time, τ_1, which is measured from the slope in the $\ln(I_{\mathrm{CL}})$ vs time transients of the p_{QW} decay curve in Fig. 11(b), is ~ 1.52 ns. τ_1 and r for emissions stemming from the stripe and the mesa regions are discussed below.

Measurements of CL spectra for the stripe region show additional features, as seen in Figs. 4, 6, and 10(b). The emissions from thin sidewalls ($\lambda = 732$ nm), thick sidewalls ($\lambda = 787$ nm), the top most GaAs layer (i.e., the QWR at $\lambda = 815$ nm), and the GaAs buffer ($\lambda = 825$ nm) are labeled as $i1$, $i2$, $i3$, and $i4$, respectively. In contrast to the gradual blue-shift of the QW emission for growth on the planar region [shown in Fig. 10(a)] as the onset time windows move from O6-O4 windows, the emission from sidewalls visibly red-shifts ~ 10 nm from the O6-O3 time windows and eventually shifts toward the 732 nm position observed in spectra measured during constant excitation (Fig. 4) and in the center of the 50 ns excitation pulse (labeled *in pulse*). Also, the relative intensity ratios of $i2/i1$, $i3/i1$, and $i4/i1$ increase for windows O6–O1. This indicates that thinner QWs on the sidewalls giving rise to $i1$ are expected to exhibit faster quantum capture times followed by the re-emission of these carriers on a time scale of a few hundred ps and thermalization into thicker QWs, the QWR, and the GaAs buffer. Dur-
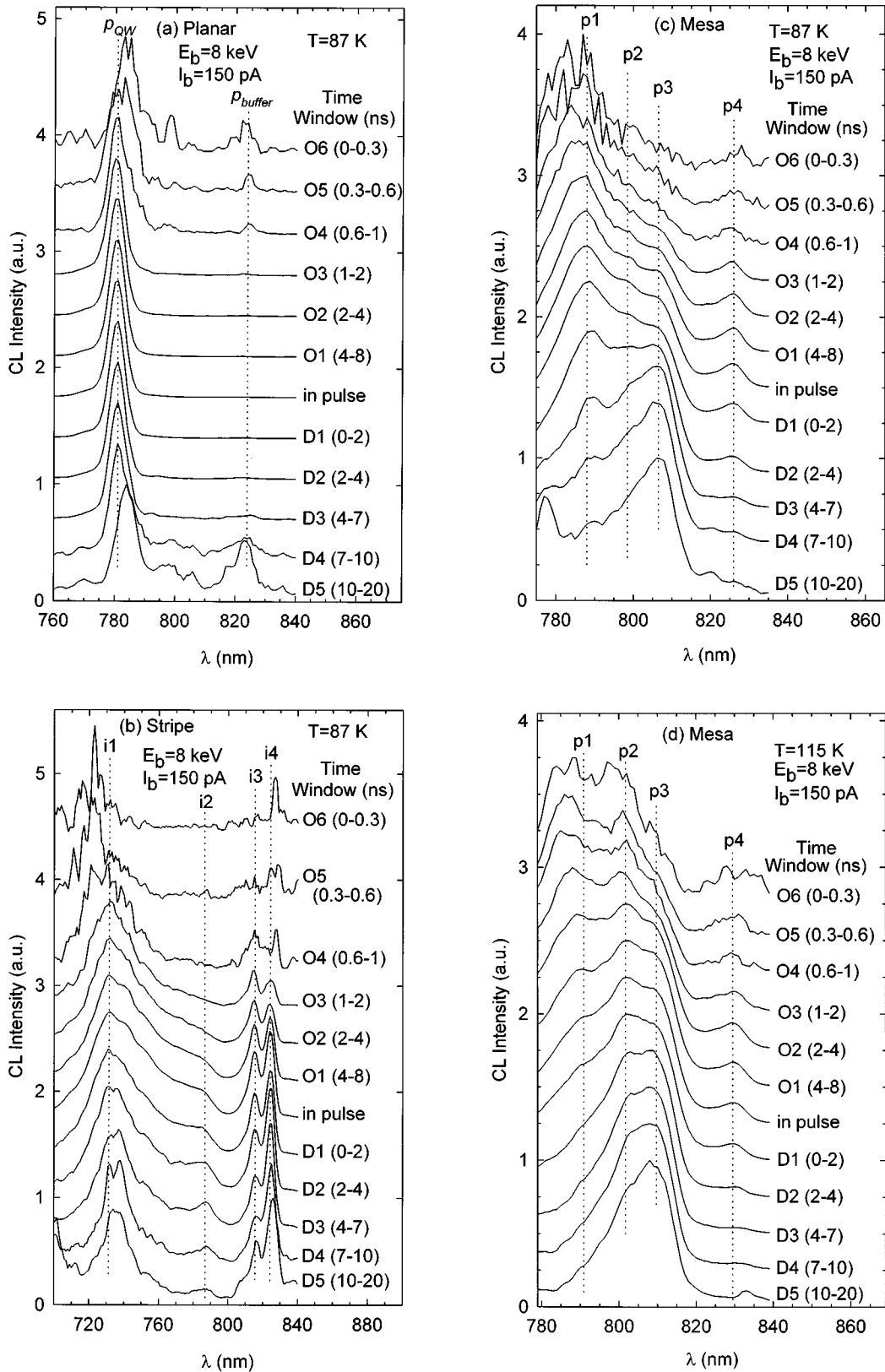
FIG. 10. Time delayed CL spectra for the (a) planar region, (b) stripe region, and (c) mesa region for $T=87$ K and (d) mesa region for $T=115$ K. The spectra are shown with various onset (Oi) and decay (Di) time windows. All spectra are renormalized to have about the same maximum peak height.

ing the decay stage (i.e., from time window D1 to D5), a further red-shift of peak $i1$ is observed and is again due to the thermal re-emission of carriers out of the thinner QWs on the sidewalls followed by the feeding of these carriers into

thicker QWs, the QWR, and the GaAs buffer region. In order to further quantify the onset rate r and decay lifetime τ_1 at different peak positions, luminescence onset and decay curves were measured and the results are shown in Fig. 12.
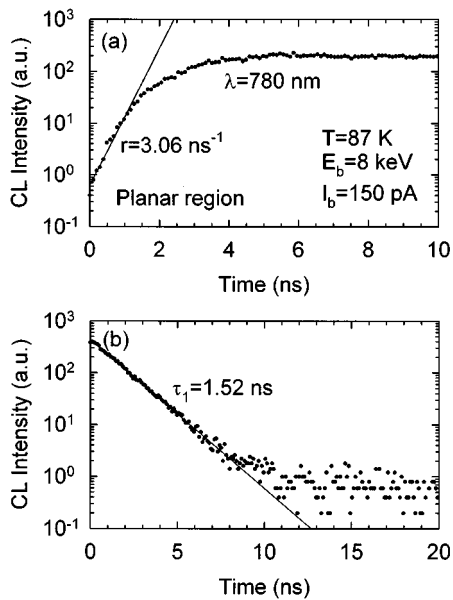
FIG. 11. CL transients for peak p_{QW} in the planar region. The onset curve is shown in (a), with a linear fit for the first ~ 1 ns yielding $r=3.06$ ns^{-1}. The decay curve (b) shows the result of a linear fit, $\tau_1=1.52$ ns, for the initial ~ 6 ns of decay.

The onset rates r for $i1$, $i2$, $i3$, and $i4$ are 2.71, 2.08, 2.16, and 2.05 ns^{-1}, respectively. The results reveal that r for $i1$ is considerably greater than that for $i2$-$i4$, further supporting the notion that thinner QWs and barriers result in faster quantum capture times. The initial decay lifetimes, τ_1, are 1.87, 2.05, 1.83, and 2.32 ns, respectively, for $i1$, $i2$, $i3$, and $i4$. τ_1 for $i2$ and $i4$ is significantly greater than that for $i1$ as a result of carrier re-emission out of thinner QWs followed by carrier relaxation into thicker QWs and GaAs buffer. However, $i3$ exhibits an initial decay lifetime τ_1 which is close to that for $i1$, thus reflecting an insignificant carrier transfer from surrounding regions into the GaAs QWR during the decay phase. This result may also be explained by the relatively short distances involved in thermalization and diffusion of carriers from thinner QWs on the sidewalls to the QWR. A reduction in carrier transfer to the QWR during the decay phase compared to the situation for the QW is attributed to the potential barriers and thinner QWs surrounding the QWR which, in this particular case, hinder the collection of carriers. Conversely, other systems have shown evidence for an enhanced carrier collection in the nanostructure, such as in the case of QWRs grown in V-shaped grooves.[21,22] The primary purpose of the thin QW sidewalls surrounding the QWR, is to serve as optical markers in this study, rather than as conduits for enhanced transport. We stress that these optical markers enabled the time-resolved CL analysis of the spectral, spatial, and temporal dependence of carrier relaxation, diffusion, and luminescence for regions in close proximity to the QWR.

Time-delayed CL spectra of the mesa region are shown in Figs. 10(c) and 10(d) for $T=87$ and $T=115$ K. A rapid capture of carriers into thinner QWs gives rise to the $p1$ feature, which is the strongest emission for the O6 time window centered at 150 ps. The CL intensity of peaks $p1$-$p4$
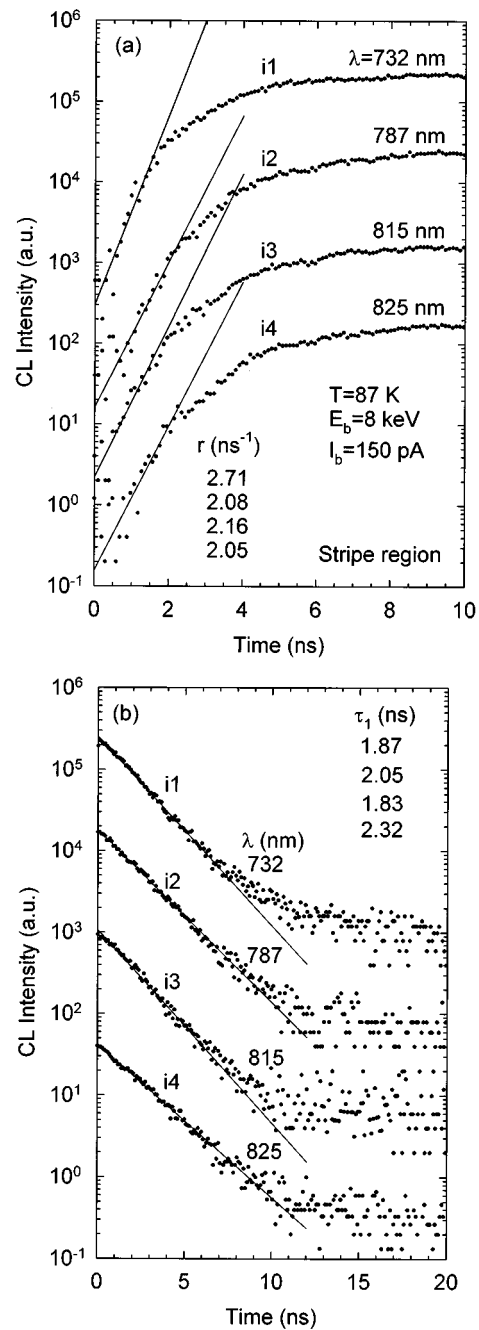
FIG. 12. CL transients for peaks $i1$-$i4$ in the stripe region. The onset (a) and decay (b) curves and the corresponding onset rates r and initial decay times τ_1 are indicated for each peak.

versus onset time is shown in Figs. 13(a) and 14(a) for temperatures of 87 and 115 K, respectively. The other features in Figs. 10(c) and 10(d), $p2$-$p4$, also grow rapidly in the 0–2 ns range. The peak intensity ratios, $p2/p1$, $p3/p1$, and $p4/p1$, as a function of onset time are shown in Figs. 13(b) and 14(b) for $T=87$ and $T=115$ K. Peak $p1$ exhibits a blue-shift of ~ 5 nm during the O6 and O5 windows (centered at 150 and 450 ps, respectively) and gradually shifts toward the 788 nm position which is observed in spectra measured during constant excitation (Fig. 4) and also in the center of the 50 ns excitation pulse [i.e., labeled *in pulse* in Fig. 10(c)]. Analogous to the findings in stripe region, the thinner QWs and
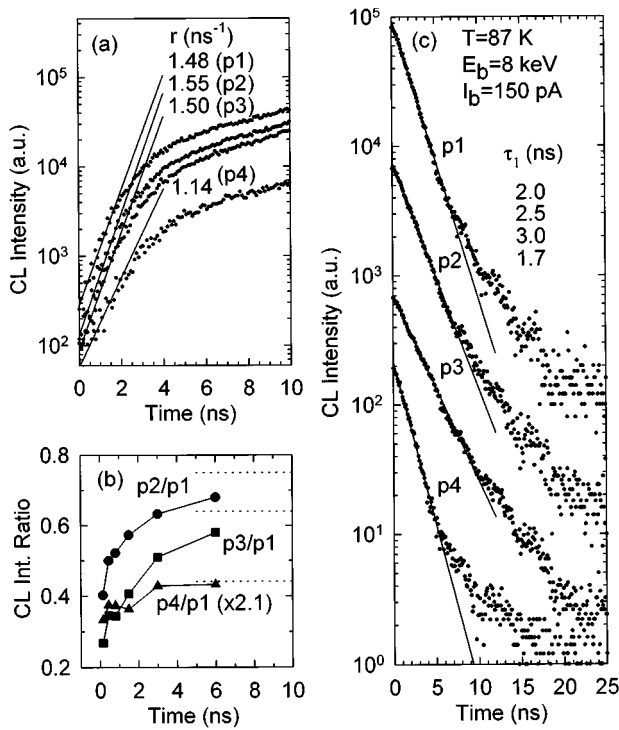
FIG. 13. CL transients for peaks *p1-p4* in the mesa region for $T = 87$ K. The onset curves and corresponding onset rates r are shown in (a). CL peak intensity ratios for *p2/p1*, *p3/p1*, and *p4/p1* are shown in (b) for various onset times from 150 ps to 6 ns. The decay curves and corresponding initial luminescence decay times, τ_1, are shown in (c).
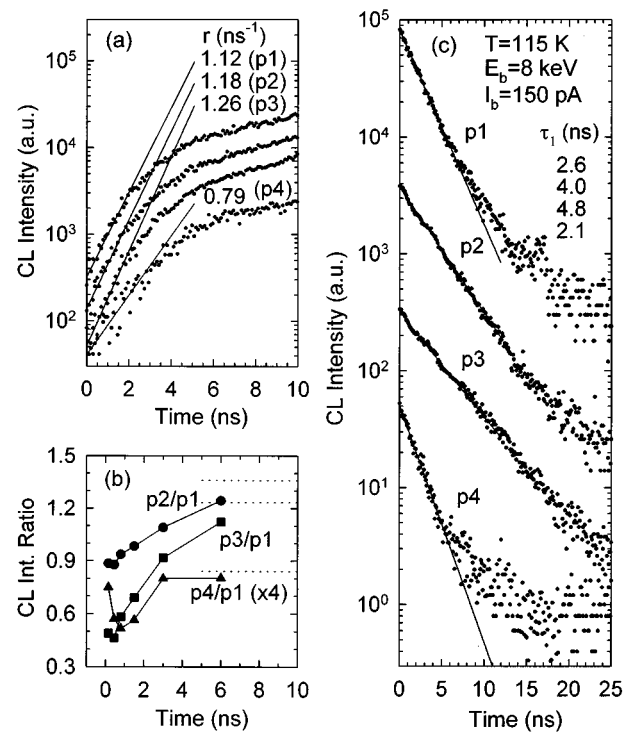
FIG. 14. CL transients for peaks *p1-p4* in the mesa region for $T = 115$ K. The onset curves and corresponding onset rates r are shown in (a). CL peak intensity ratios for *p2/p1*, *p3/p1*, and *p4/p1* are shown in (b) for various onset times from 150 ps to 6 ns. The decay curves and corresponding initial luminescence decay times, τ_1, are shown in (c).

barriers comprising emission *p1* are expected to exhibit the faster quantum capture times, and subsequent re-emission of these carriers on a time scale of a few hundred ps and thermalization into the thicker QWs comprising *p1* give rise to the gradual redshift observed for windows O6 to O1. Likewise, these carriers are also able to thermalize and diffuse over distances of ~ 0.1–0.5 μm to the thicker QWs giving rise to peaks *p2*, *p3*, and *p4*. These large distances are reflected in the relatively slow onset rates shown in Figs. 13(a) and 14(a). The slower rates for *p4* reflects the larger distances from the sidewalls (~ 0.5 μm) that hot carriers must traverse before recombining in the thick 525 ML GaAs layers. During the decay stage of the luminescence, a further red-shift of peak *p1* occurs and a continuous increase of the CL intensity ratios *p2/p1* and *p3/p1* are detected in the D1-D5 windows. As shown in Fig. 13(c), τ_1 increases in the sequence 2.0, 2.5, and 3.0 ns, respectively, for peaks *p1*, *p2*, and *p3*. For $T = 115$ K, this same sequence is 2.6, 4.0, and 4.8 ns. In comparing results for the two temperatures in Figs. 13 and 14, the onset rates and decay times increase and decrease, respectively, as the temperature is lowered. These results are expected as a result of a reduced reemission of carriers from the sidewall QWs as the temperature is lowered, yielding more rapid carrier equilibration rates. Likewise, the slower decay of *p3* relative to *p1* and *p2* is due to an enhanced thermal reemission of carriers in thinner QW sidewalls comprising *p1* and *p2* which continuously feed the larger GaAs layers represented by the *p3* feature, as the system proceeds towards equilibrium.

In comparing the dimensionality of the size-reducing growth on the carrier capture and relaxation kinetics, the onset rates, r, and initial decay lifetimes, τ_1, for aforementioned luminescence peaks in planar, stripe, and mesa regions are summarized in Table I for $T = 87$ K. The average luminescence onset rate decreases and initial decay lifetime increases as the dimensionality of the system reduces from 2D to 0D (i.e., QW to QB). These results demonstrate that thermalization and diffusive transport of hot carriers from surrounding barrier regions can impact the lifetime and carrier collection in nanostructures, such that the effect is greatest for the lowest dimensionality nanostructure, the QB. We stress these results are characteristic of nanostructures grown with a size-reducing technique so that the average areal density of the nanostructure is sufficiently low to permit non-interacting QBs and QWRs. That is, in our samples, all carriers generated within a diffusion length of the nanostructure region can only diffuse to one nanostructure.

TABLE I. Onset rates, r, and initial decay lifetimes, τ_1, for various luminescence peaks in planar, stripe, and mesa regions.

	Onset rate r (ns^{-1})				Initial decay lifetime τ_1 (ns)			
Planar	p_{QW} 3.06				p_{QW} 1.52			
	i1	*i2*	*i3*	*i4*	*i1*	*i2*	*i3*	*i4*
Stripe	2.71	2.08	2.16	2.05	1.87	2.05	1.83	2.32
	p1	*p2*	*p3*	*p4*	*p1*	*p2*	*p3*	*p4*
Mesa	1.48	1.55	1.50	1.14	2.0	2.5	3.0	1.7

Lin *et al.*

IV. CONCLUSION

In conclusion, the kinetics of carrier relaxation in GaAs/ AlGaAs quantum boxes and wires fabricated using size reducing growth have been examined with time-resolved CL. The data revealed that thermal re-emission from thin sidewall QWs and diffusion plays an important role in determining the kinetics of carrier relaxation and the onset and decay of luminescence. Hot carriers resulting from thermal re-emission out of the surrounding thin QWs contribute to the total number of carriers collected by the QBs and, to a lesser extent by the QWRs, thereby giving rise to a relatively slow onset and decay of luminescence at elevated temperatures. Due to the differences in the growth and cation migration rates on different facets, growth of GaAs/AlGaAs layers on the patterned GaAs(001) substrate resulted in regions of 2D and 3D confined GaAs volumes in stripe and mesa regions giving rise to the QWRs and QBs, respectively. The thinner sidewall QWs in this study have conveniently served as *optical markers*, in addition to their intended purpose of structural markers, thereby providing key signatures in the wavelength and time domain that allow for a visualization of the carrier relaxation. It is anticipated, therefore, that a suitable choice of cladding layers during future designs of sizereducing growth will enhance the efficiency of carrier collection into QBs and QWRs residing just below the pinch-off region. In comparing the time-resolved luminescence curves in the three structures examined in this study, we find that the averaged onset and initial decay rates of luminescence decrease in the sequence: the planar (no patterning), stripe (QWRs), and mesa (QBs) regions. These results suggest that (i) the carrier relaxation kinetics can be controlled by proper choice of the structural design in the size reducing growth and (ii) the total rate of carrier relaxation comprising reemission, diffusion, and thermalization of carriers is considerably reduced as the dimensionality of the system reduces from 2D to 0D.

[1] *Nanostructure and Mesoscopic Systems*, edited by W. Kirk and M. A. Reed (Academic, New York, 1992).

[2] A. Madhukar, K. C. Rajkumar, and P. Chen, Appl. Phys. Lett. **62**, 1547 (1993), and references therein.

[3] K. C. Rajkumar, A. Madhukar, K. Rammohan, D. H. Rich, P. Chen, and L. Chen, Appl. Phys. Lett. **63**, 2905 (1993).

[4] A. Konkar, K. C. Rajkumar, Q. Xie, P. Chen, A. Madhukar, H. T. Lin, and D. H. Rich, J. Cryst. Growth **150**, 311 (1995).

[5] E. Kapon, M. C. Tamargo, and D. M. Hwang, Appl. Phys. Lett. **50**, 347 (1987).

[6] E. Kapon, D. M. Hwang, and R. Bhat, Phys. Rev. Lett. **63**, 430 (1989).

[7] D. Leonard, M. Krishnamurthy, C. M. Reaves, S. P. Denbaars, and P. M. Petroff, Appl. Phys. Lett. **63**, 3203 (1993).

[8] M. Grundman *et al.*, Phys. Rev. Lett. **74**, 4043 (1995).

[9] Q. Xie, A. Madhukar, P. Chen, and N. P. Kobayashi, Phys. Rev. Lett. **75**, 2542 (1995).

[10] K. C. Hsieh, J. N. Baillargeon, and K. Y. Cheng, Appl. Phys. Lett. **57**, 2244 (1990).

[11] K. Y. Cheng, K. C. Hsieh, and J. N. Baillargeon, Appl. Phys. Lett. **60**, 2892 (1992).

[12] D. H. Rich, H. T. Lin, A. Konkar, P. Chen, and A. Madhukar, Appl. Phys. Lett. **69**, 665 (1996).

[13] D. H. Rich, A. Ksendzov, R. W. Terhune, F. J. Grunthaner, B. A. Wilson, H. Shen, M. Dutta, S. M. Vernon, and T. M. Dixon, Phys. Rev. B **43**, 6836 (1991).

[14] J. S. Weiner, D. S. Chemla, D. A. B. Miller, H. A. Haus, A. C. Gossard, W. Wiegmann, and C. A. Burrus, Appl. Phys. Lett. **47**, 664 (1985).

[15] P. C. Sercel and K. J. Vahala, Appl. Phys. Lett. **57**, 545 (1990).

[16] P. C. Sercel and K. J. Vahala, Phys. Rev. B **44**, 5681 (1991).

[17] Y. Tang, H. T. Lin, D. H. Rich, P. Colter, and S. M. Vernon, Phys. Rev. B **53**, R10501 (1996).

[18] B. Deveaud, J. Shah, T. C. Damen, and W. T. Tsang, Appl. Phys. Lett. **52**, 1886 (1988).

[19] U. Jahn, J. Menniger, R. Hey, and H. T. Grahn, Appl. Phys. Lett. **64**, 2382 (1994).

[20] K. Rammohan, H. T. Lin, D. H. Rich, and A. Larsson, J. Appl. Phys. **78**, 6687 (1995).

[21] J. Christen, M. Grundmann, E. Kapon, E. Colas, D. M. Hwang, and D. Bimberg, Appl. Phys. Lett. **61**, 67 (1992).

[22] J. Christen, E. Kapon, E. Colas, D. M. Hwang, L. M. Schiavone, M. Grundmann, and D. Bimberg, Surf. Sci. **267**, 257 (1992).

J. Appl. Phys., Vol. 81, No. 7, 1 April 1997

Lin *et al.*   3195